

Published by Fusion Energy Division, Oak Ridge National Laboratory Building 5700 P.O. Box 2008 Oak Ridge, TN 37831-6169, USA

Editor: James A. Rome Issue 121 August 2009

E-Mail: jar@ornl.gov Phone (865) 482-5643

On the Web at http://www.ornl.gov/sci/fed/stelnews

Magnetic field shaping with high-temperature superconducting monoliths

1. Introduction

Stellarators offer substantial physics advantages for fusion reactors, both in the near term as experimental facilities, and in the long term as commercial fusion reactors [1,2,3,4]. Stellarators are attractive for reactors because they do not have disruptions, are truly steady state, and have high beta limits. On the other hand, engineering of stellarators is challenging, in particular, the design of the magnetic field coils and the diverter [5,6].

In this article and a forthcoming paper [7], a novel method is investigated to simplify the magnetic field coils. The use of monolithic high-temperature superconductor (HTS) for field shaping in stellarators and tokamaks is presented. The basic concept investigated in this paper is to use a relatively simple coil set that generates a background magnetic field, and to use HTS monoliths to shield/shape the magnetic field to the desired configuration.

The properties of presently available monolithic HTS are described in Section 2, as is the physical model used to describe the superconducting monoliths. Yttrium barium copper oxide (YBCO) has excellent properties, operating at elevated temperatures (> 10 K). High-field, cryostable, highly complex magnetic field topologies can be generated using this material. The diamagnetic properties of the bulk HTS material can be used to provide simple mechanisms for field shaping.

Section 3 describes the design issues relevant to tokamak magnets using single crystal or highly textured YBCO monoliths. Engineering constraints, such as stresses in the superconducting monoliths, support, quench protection, superconducting stability of the monoliths, and required external support structure are described.

Section 4 briefly touches on the application of this approach to stellarators.

2. HTS monoliths

A. Properties and availability

There is a small program worldwide to develop monoliths of HTS material. During the initial phases of high-temperature superconductivity, the only materials that were available were bulk materials. This was the case for Bismuth-2 Strontium-2 Calcium Copper-2 oxide (B-2212) and YBCO. Wires were initially made from B-2212, but this effort was dropped because of the material's relatively poor superconducting properties at 77 K.

Presently, both B-2212 and YBCO are available. BSCCO-2212 is more developed, because of its application as a current lead, and more recently, as a component of fault

In this issue . . .

Magnetic field shaping with high-temperature superconducting monoliths

Nonlinear simulation of a collapse event in LHD

All Wendelstein 7-X coils successfully tested

All opinions expressed herein are those of the authors and should not be reproduced, quoted in publications, or used as a reference without the author's consent.

Oak Ridge National Laboratory is managed by UT-Battelle, LLC, for the U.S. Department of Energy.

current limiters. This material is available from Nexans, as rods, cylinders, or plates. While its properties are lackluster at 77 K, they are very good at 20–30 K.

Bulk YBCO is being developed mainly as a material to be used in bearings, in the USA (Boeing), Europe (Nexans), and Japan (ISTEC), among others. The characteristics of this material are nothing less than spectacular at temperatures up to 60–65 K. YBCO has limited current density capabilities at 77 K, good enough for tapes, but not for high-field magnet applications, which need to be operated in subcooled liquid nitrogen.

The most impressive performance of YBCO pucks has been a 17 T magnet at 29 K without a background field [8]. For B-2212, the MIT group has built a 3 T magnet at 4 K, and a 1 T insert in a 19 T background [9].

These materials are available at costs of 15 e/cm^2 (150 ke/m^2).

B. Modeling of HTS bulk material

The interaction of HTS bulk material with magnetic fields is very nonlinear and complex. In this section two methods that simplify the complex behavior are described. These methods are used in the remainder of the paper to analyze interactions between tiles of HTS monoliths and the magnetic field.

Using the simple Bean model of superconductivity, the HTS monoliths are assumed to be at critical current density. As the external field is raised, currents are generated on the surface of the monoliths to prevent penetration of the field to the bulk. The current density is a function of the temperature of the monolith and the local applied field. The "skin" current thickness increases with increasing magnetic field. As the field decreases, edge currents flow in the reverse direction on the surface, locally trapping some magnetic field.

If the current density capability of the monoliths is large and the thickness of the skin currents is small compared with the size of the monoliths, the monoliths can be described as "diamagnetic" elements.

Two methods have been used to describe the diamagnetic model of the HTS monoliths. The first assumes that the magnetic field is parallel to all surfaces of the monolith. The second one assumes that the magnetic permeability μ of the HTS monoliths is very small. While either method works, the second one is easier to implement, as applying the boundary conditions to all surfaces of the monoliths is time consuming.

We have used $\mu = 0.001$ in the remainder of this paper to describe the HTS monoliths.

C. Estimate of forces/currents in HTS monolith

The interaction between HTS monoliths and magnetic field can be divided into two effects. The first is the surface currents that exclude the external magnetic field from the superconductor. It is straightforward to estimate the value of these currents. The surface current density excited by the presence of the field is simply

$$K = B/\mu_0$$

where B is magnetic field external to the surface of the monoliths. The critical current densities of YBCO are on the order of 10^9 – 10^{10} A/m². Thus, to expel a field of 5 T, the thickness of the current carrying layer is less than 0.01 m (1 cm). It is expected that the value of the field outside the surface of the monolith is comparable to the applied field, B_0 (the assumption being that the main effect of the HTS monoliths is to "globally" turn the direction of the magnetic field). These currents exist even if the wide surface of the monolith is aligned with the magnetic field, in which case one would not expect the direction of the field to be modified.

The second effect is due to the interception of fields perpendicular to the wide surface of the monolith. Assuming that the tiles have a dimension of the average diameter of the tiles, the magnetic moment generated by the presence of the monolith is

$$m \sim \frac{\pi^2}{4\mu_0} B_0 a^3 \cos \delta$$

where δ is the angle between the main normal to the monolith and the applied magnetic field.

The main difficulty with these simple models arises because of interactions with adjacent tiles, which generate local magnetic fields. This makes it necessary to solve the problem using multidimensional models.

The torque that a monolith will experience in the presence of an externally applied magnetic field B_0 is on the order of

$$\tau = \boldsymbol{m} \times \boldsymbol{B}_0 \sim \frac{\pi^2}{4\mu_0} B_0^2 a^3 \sin \delta \cos \delta$$

The forces/torques are very large and must be supported. In order to quantify the forces, the full multidimensional effects must be calculated.

D. Effect of gaps between monoliths

The magnetic field does not have to follow the main surface of the superconducting monoliths in the gaps between monoliths; that is, the magnetic field can "escape" through these regions.

One option to avoid the effect of the gaps between monoliths is to stack multiple layers of monoliths, such that they

are staggered. Although the field can still escape through a gap, it is intercepted by the monolith behind.

The impact of the staggered layer of monoliths also requires numerical calculation. This is described in the next section.

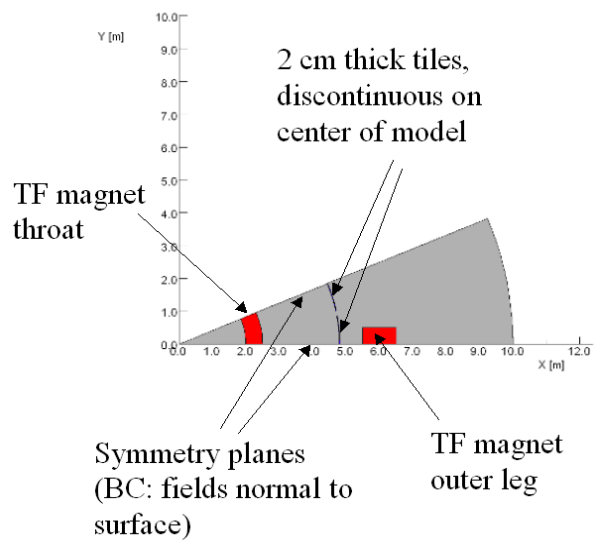


Fig. 1. Schematic of geometry used to calculate the effect of multiple HTS monoliths on the toroidal field ripple in tokamaks.

3. Use of HTS monolith for toroidal field ripple cancellation

The quantitative work was complex. Simpler geometries were investigated and are reported here. A simple geometry using helical coils for a cylindrical configuration proved to provide none of the simplifications that a two-dimensional (2D) model would have. That is, the helical geometry still needs a 3D model for analysis.

In the remainder of this section we describe calculations that are directly relevant to tokamaks. It is possible to build a simple 2D model representing the use of monoliths for ripple control.

The simple model is shown in Fig. 1. The model uses a toroidal field (TF) system with only 8 coils, with relatively large ripple. The outer legs of the coils are at 6 m. The ripple calculations for these coils are performed at a radius of 4 m.

The throat of the magnet is assumed to be continuous, with discrete legs in the outboard side. The symmetry of the problem was used to decrease the size of the required mesh. The planes with boundary conditions of normal magnetic fields are shown. It is assumed that the model is 2D, with coils extending in the direction out of the plane.

Thus, the model is directly applicable to the midplane region of tokamaks.

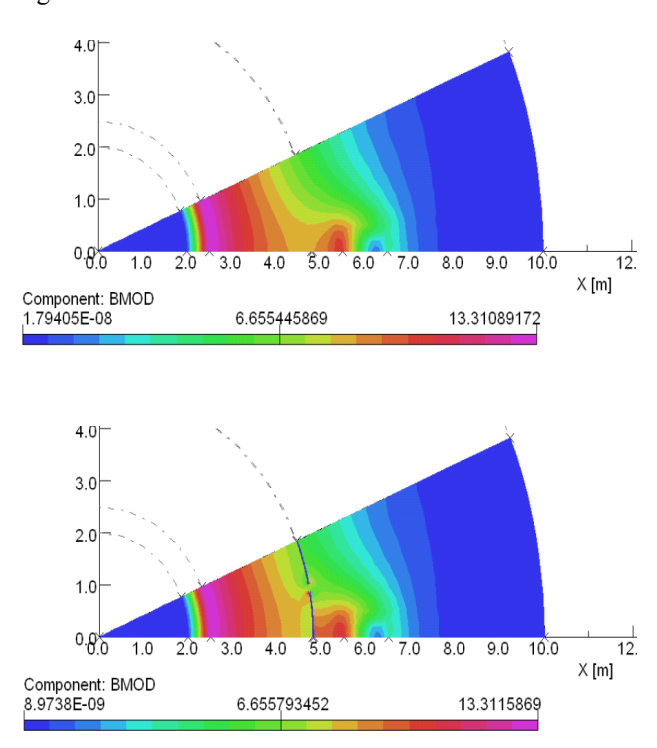


Fig. 2. (Contours of constant magnetic field for the tokamak case with 8 coils. Top: no HTS monoliths (base case). Bottom: 16 HTS monoliths.

A. Single layer of monoliths with 16 azimuthal monoliths

The commercial code VectorFields from Opera-2D software is used to model this system. The problem is solved with multiple adaptations of the grid until 0.1% accuracy of the solution is achieved.

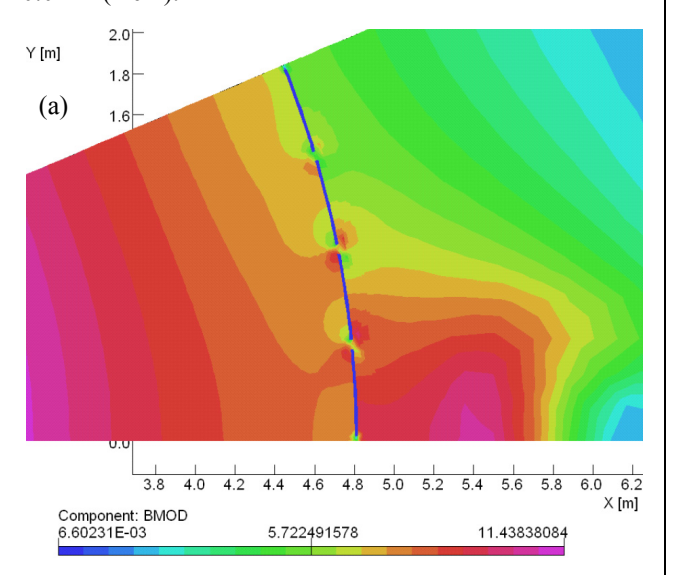
Contours of constant magnetic field are shown in Fig. 2. The top shows the results for no monoliths, while the bottom shows the results for one layer with large tiles. The case shown in the bottom part of Fig. 2 has 16 monoliths, with the centerline of one of the monoliths corresponding to the shadow of the TF coils. Both a substantial perturbation of the field in the region of the tiles, and the effect of the gap are readily seen. As described above, the field tends to "squeeze out" between the monoliths.

The effects of smaller tiles and multiple layers are described in the next section.

B. Multiple layers

There are 8 tiles between each pair of TF coils, or 64 tiles around the device. For the geometry chosen for the example, the monoliths are about 30 cm in width. In all cases, the thickness of the monoliths is assumed to be 0.02 m (2 cm).

The first layer of monoliths occurs at $4.8 \, \text{m}$, and each subsequent layer is placed at $5 \, \text{cm}$ intervals, that is, the separation between layers is $0.03 \, \text{m}$ ($3 \, \text{cm}$). The gap between the tiles has been varied from about $0.01 \, \text{m}$ ($1 \, \text{cm}$) to about $0.04 \, \text{m}$ ($4 \, \text{cm}$).



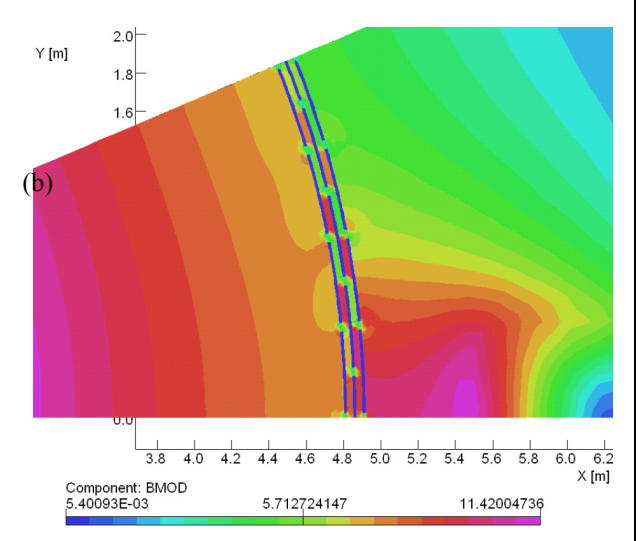


Fig. 3. Contours of constant magnetic field (a) for the case of a single layer of 0.3 m monoliths and (b) for the case of 3 layers of monoliths with 3 cm between layers.

Figure 3 shows the resulting field profiles for the cases of 1 and 3 layers of 0.3 m monoliths. It is interesting to note the dark regions of high-intensity magnetic field between some tiles. The field is not prevented from penetrating between tiles by the presence of monoliths downstream, but instead "squeezes out" between the tiles in a staircase-like pattern. However, it is clear that the magnetic field ripple has been decreased, as the contours of constant magnetic field look more axisymmetric.

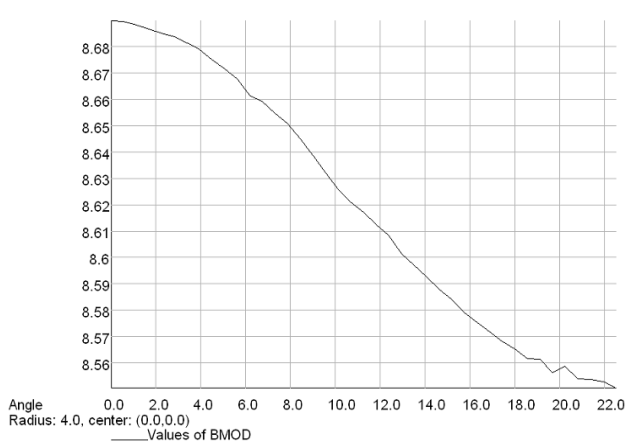


Fig. 4. Magnetic field magnitude as a function of the toroidal angle for the case of 3 layers of 0.3 m monoliths, corresponding to the case shown in Fig. 3(b).

Figure 4 shows the magnetic field along an arc at 4 m, along the toroidal direction. Shown in Fig. 4 is a half-distance between coils, using the symmetry properties of the model. The field is sinusoidal. No higher harmonics are visible in the field, showing that the local field from the individual monoliths has been "washed out."

Corresponding values of peak-to-peak ripple are shown in Fig. 5 as a function of the number of layers. The field ripple is about 7% with no correction by the monoliths, and decreases exponentially as the number of layers increases. The exponent is about 0.5. Between 4 and 5 layers are required in order to reduce the ripple to <1%.

Ripple at R = 4 m

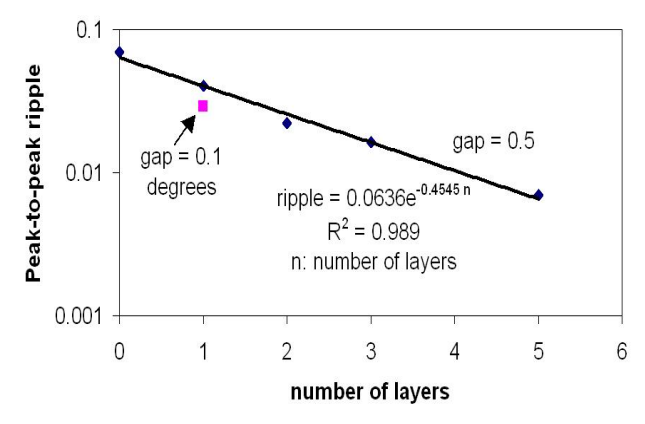


Fig. 5. Peak-to-peak ripple at 4 m as a function of the number of layers, for two cases of gaps between monoliths.

Also shown in Fig. 5 is the ripple for the case with a smaller gap between monoliths. In the results up to now the toroidal gap between monoliths has been 0.5°, corre-

sponding to about 0.04 m between tiles. The point indicated with 0.1° between monoliths in Fig. 5 corresponds to about 0.008 m between tiles.

Although the results are for infinitely long monoliths, the results are expected to be relevant even for tiles of limited extent in the poloidal direction.

The thickness of the current-carrying layer can be determined from these results. It is on the order of 1 cm, so the assumption of perfectly diamagnetic monoliths, although not exact, does provide good insight into the performance of the monoliths for shaping fields in toroidal geometries.

4. Stellarator geometry

The complex geometry of the stellarator is presently being investigated using the same model. Figure 6 shows the model that is being implemented in VectorFields.

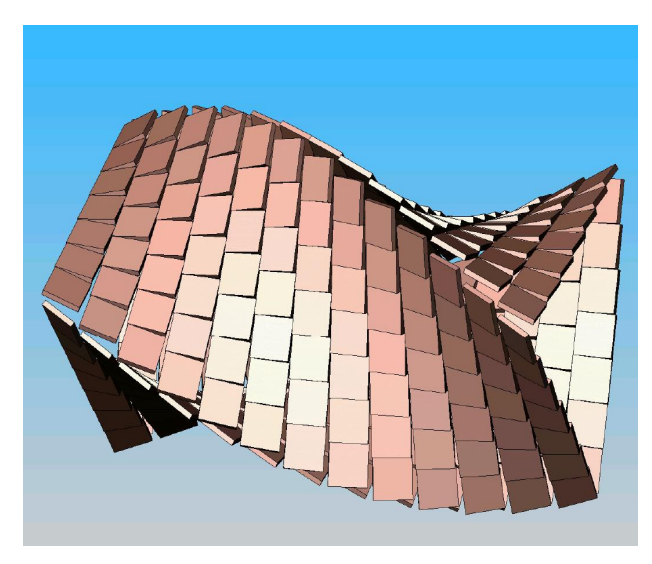


Fig. 6. Helical geometry with tiles along three surfaces, for future investigation of field shaping.

Acknowledgment

Suggestions and feedback from Hutch Neilson are appreciated.

L. Bromberg, J.V. Minervini, J.H. Schultz Plasma Science and Fusion Center Massachusetts Institute of Technology Cambridge MA, USA

E-mail: brom@psfc.mit.edu

A. Boozer, T. Brown, P. Heitzenroeder, and M. Zarnstorff Princeton Plasma Physics Laboratory Princeton University, Princeton NJ, USA

References

- [1] C. D. Beidler, E. Harmeyer, F. Herrnegger, et al., "The Helias reactor HSR4/18," Nucl. Fusion, **41** (2001) 1759
- [2] A. Sagara, and O. Motojima, "LHD-type reactor design studies," Fusion Technol., **34** (1998) 1167–73.
- [3] M. Wanner, J.-H. Feist, H. Renner, J. Sapper, F. Schauer, H. Schneider, V. Erckmann, H. Niedermeyer, W7-X Team, "Design and construction of Wendelstein 7-X," Fusion Eng. Des. 56–57 (2001) 155–162.
- [4] B. E. Nelson, L. A. Berry, A. Brooks, et al., "Design of the National Compact Stellarator Experiment (NC-SX)." Fusion Eng. Des. 66–68 (2003) 169-174.
- [5] F. Najmabadi and A. R.Raffray, "The ARIES-CS compact stellarator fusion power plant", Fusion Sci. Technol. 54 (2008) 655–72.
- [6] X. R. Wang, A. R. Raffray, L. Bromberg, J. H. Schultz, L. P. Ku, J. F. Lyon, et al., "ARIES-CS Magnet Conductor and Structure Evaluation," Fusion Sci. Technol., 54 (2008) 818–837.
- [7] T. Brown, L. Bromberg, M. Cole "Results of compact stellarator engineering trade studies," Symposium of Fusion Engineering, San Diego, June 2009.

[8]

- [9] M. Tomita and M. Murakami, "High-temperature superconductor bulk magnets that can trap magnetic fields of over 17 Tesla at 29 K," Nature 421 (2003) 517–20.
- [10] L. Bromberg, private communication (unpublished).

Nonlinear simulation of a collapse event in LHD

1. Introduction

Controlling the collapse phenomena which take place in toroidal experiments is one of the key issues for the development of fusion sciences. Such collapse phenomena usually proceed on a magnetohydrodynamic (MHD) time scale, sometimes accompanied by precursory oscillations, and are in general harmful to confinement. Because the collapse phenomena are governed by highly nonlinear processes, it is necessary to make use of nonlinear numerical simulation techniques.

In recent high-performance helical experiments such as the super-dense core (SDC) state of the Large Helical Device (LHD) [1], a collapsing event with an abrupt flushing of the core density has been observed under certain situations. This event is termed a core density collapse (CDC) [2]. CDCs are typically observed in the reheating stage during which the plasma beta gradually increases after a pellet injection series. The crash phase of the CDCs is characterized by a rapid fall of the central density and its expulsion toward the edge. CDCs are sometimes accompanied by precursors in the outer region [3]. Further increase of the plasma beta is limited by the CDC in some cases. The CDC is phenomenologically understood at present, whereas the detail mechanism, in particular the nonlinear dynamics of the crash phase, has not yet been clarified.

In this study, we aim at providing a qualitative understanding of the nonlinear dynamics of a collapse phenomenon in a heliotron plasma with a large pressure gradient (characteristic of the SDC state of LHD) by means of a nonlinear MHD simulation.

2. Simulation model

The governing equations for the simulation are the nonlinear, resistive, compressive equations,

$$\frac{\partial \rho}{\partial t} = -\nabla \bullet (\rho \mathbf{v}), \tag{1}$$

$$\frac{\partial}{\partial t}(\rho \mathbf{v}) = -\nabla \bullet (\rho \mathbf{v} \mathbf{v}) - \nabla p + \mathbf{J} \times \mathbf{B} + \mu \left[\nabla^2 \mathbf{v} + \frac{1}{3} \nabla (\nabla \bullet \mathbf{v}) \right]$$

$$+\mu \left[\nabla^2 \mathbf{v} + \frac{1}{3} \nabla (\nabla \bullet \mathbf{v}) \right], \tag{2}$$

$$\frac{\partial B}{\partial t} = -\nabla \times \mathbf{E} \,, \tag{3}$$

$$\frac{\partial p}{\partial t} = -\nabla \bullet (p\mathbf{v}) - (\gamma - 1)(p\nabla \bullet \mathbf{v} + \eta j^2), \qquad (4)$$

where the density ρ , fluid velocity \mathbf{v} , magnetic field \mathbf{B} , and the pressure p are developed. The current density j and the electric field \mathbf{E} are evaluated by

$$\mathbf{j} = \nabla \times \mathbf{B}, \tag{5}$$

$$\mathbf{E} = -\mathbf{v} \times \mathbf{B} + \eta \mathbf{j} \,. \tag{6}$$

In Eqs. (1)–(6), the dissipation terms are included as the resistivity η and the viscosity μ . These terms are assumed to be uniform constants for simplicity. All spatial derivatives are expressed numerically using a fourth-order central difference scheme, and together with the time integration were solved using the fourth-order Runge-Kutta method. The simulations are executed in full toroidal three-dimensional geometry using the helical-toroidal coordinate system that is used in the HINT code [4]. The helical period h is set at 10/2 to follow the LHD configuration. The numbers of the numerical grid are 62×146 for the poloidal cross section, and 500 for the toroidal direction. The simulation geometry includes the region out of the separatrix, which is treated as an initially biased low-pressure plasma.

The initial condition for the simulation is given by the numerical solution of the HINT2 code [5]. In particular, the profile of the equilibrium models an average experimental configuration of LHD during outward-shifted operation with an SDC. Note that the unit of the time of the simulation roughly corresponds to 1 s of the experiment.

The simulation starts by adding tiny random perturbations to the velocity components of the initial equilibrium. Then, the spontaneous time development of the MHD system is solved by vector-parallel calculation on a supercomputer.

3. Simulation result

For high resistivity, $\eta = 10^{-4}$, the system tends to be unstable for some resistive instabilities. Al-though such unrealistically high resistivity may exaggerate the linear growth rate of the resistive instability modes compared to the experiments, these simulation results can help us obtain a basic understanding of the nonlinear behavior of the resistive modes. The structure of the linear eigenmode is shown in Fig. 1 with the contour of the perturbations in the pressure at the horizontally elongated poloidal cross section. The mode component is poloidally localized in the outer region with the intermediate $(m \sim 15)$ components, where m is the poloidal mode number. Such a ballooninglike nature is seen at any toroidal location. Moreover, the mode structure is almost identical for all of the horizontally elongated plane. This implies that the low-n components, where n is the toroidal mode number, are not so significant in this case.

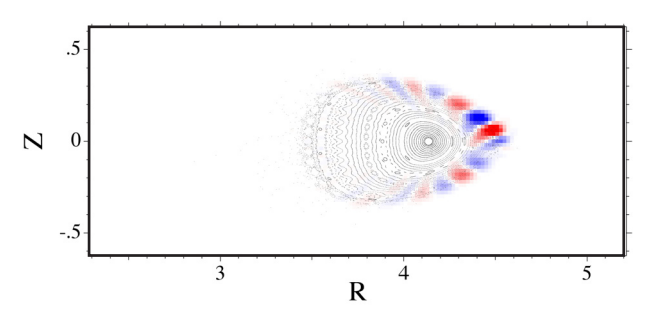


Fig. 1. The linear eigenmode structure. Perturbations in the pressure are plotted with color contours. The puncture plot of magnetic field for the initial condition is also shown.

As the amplitude of the perturbations becomes large, the configuration is deformed spontaneously into a visible scale, and the growth is saturated. The time development of the overall system is plotted with the change in total kinetic energy in Fig. 2. One can see that the growth and the relaxation of the instability repeat three times in about $t = 500\tau_A$. The corresponding change in the pressure profile shows disordering by the instability in the edge region. Moreover, the central pressure also drops as time goes on. This behavior is clearly shown in Fig. 2 in the trace of maximum pressure. The most rapid drop in pressure is observed at around $t = 335\tau_A$. The system reaches its final relaxed state just after this rapid pressure drop. In the final state, the pressure profile forms a wide tail in the peripheral region.

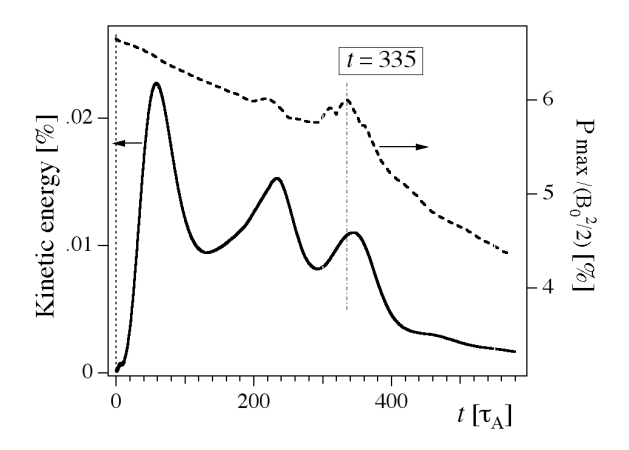


Fig. 2. Time development of the total kinetic energy normalized by the initial plasma thermal energy and the maximum pressure.

The collapsing process is more clearly visualized by a two-dimensional contour plot of the pressure profile in a horizontally elongated poloidal cross section, as shown in Fig. 3. The structure is destroyed in the peripheral region, reflecting the linear eigenmode structure. The convection motions of the eigenmodes form a number of finger-like structures in the unstable region. The disordered region is

extended inward. However, the bulk of the plasma is not displaced away, despite the rapid fall at $t \sim 335\tau_A$. This is a remarkable contrast to our previous simulation for the spherical tokamak case [6], where the rapid fall of the core pressure is caused by a secondary induced internal low-m/n instability.

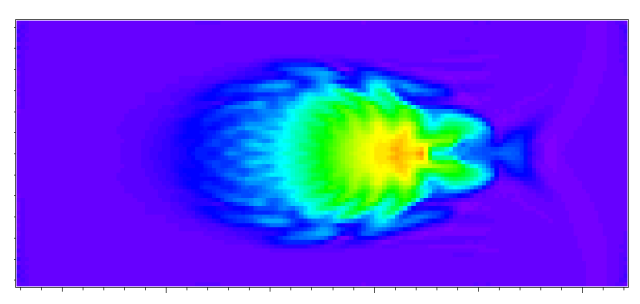


Fig. 3. Deformation of the pressure profile on a horizontally elongated poloidal cross section at $t = 335\tau_{A}$.

The period of the core pressure fall at around $t = 335\tau_{\rm A}$ is characterized by some qualitative transitions of the system. The most salient feature of this period is the disordering of the magnetic field structure. The system maintains nested flux surfaces in the core region before $t = 335\tau_{\rm A}$, but some of these flux surfaces are abruptly lost at around $t = 335\tau_{\rm A}$. As the core pressure drop ends, the flux surfaces gradually reappear. Such a disordered magnetic structure can cause a flattening of the pressure profile in a wide region due to the parallel equilibration motion of MHD. Therefore, the disordering of the magnetic structure can be considered to be the direct cause of the core pressure collapse.

This insight can be supported by another observation of the simulation result concerned with the plasma flow structures. To find the place where the plasma loss due to this mechanism occurs extensively, the internal energy flux |pV| is plotted in Fig. 4(a) using color contours on top of the pressure profile, which is indicated by the gray contours. One can see that such plasma outlets are mainly located at the roots of the fingers. Another simple analysis shows that the direction of the energy flux is almost parallel to the magnetic field. The neighboring magnetic structure is also shown in Fig. 4(b). The magnetic flux surfaces are hard to find except in the regions between the islands or their ruins. In Fig. 4(b), one can see a couple of wellformed surfaces at R = 4.24 m and 4.30 m on the equator (Z=0), putting the ruins of the t=2/3, 5/8, and 4/7 islands between them, with the outlets corresponding to the disordered region. Thus, within the MHD framework, the magnetic and flow structures show that the core pressure can be expelled away through the disordered or reconnected field lines. Note that the spots of the outlets are seen apart from the original linear eigenmode ones, which are indicated with the red and blue contours in Fig. 4.

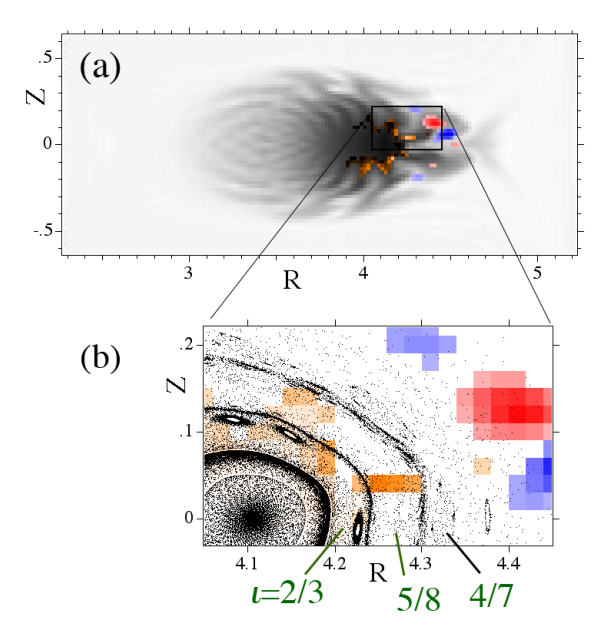


Fig. 4. Poloidal profiles of the plasma pressure energy flux at $t = 335\tau_A$. (a) Contours of the absolute value of the energy flux |pV| (orange), perturbations in the pressure in the linear eigenmode (red and blue), and net pressure (gray). (b) Magnification of the box in (a) without the pressure but with the puncture plot of the magnetic field lines. The original locations of the rational surfaces for t = 2/3, t = 5/8, and t = 4/7 are also specified (green).

4. Discussion and summary

The simulation results described here can be compared in several ways with the experimental observations of the CDC in LHD. First, the time scale of the crash phase of the CDC is of the order of sub-milliseconds, which is comparable to the whole relaxation process of the simulation result. As mentioned above, the resistivity for the simulation is assumed to be much larger than a realistic one, and the linear growth of the resistive modes may thus appear to be more rapid. However, since the nonlinear behavior (including the loss mechanism of the core pressure) is dominated by the convection term of the MHD fluid, the time scale should not be much affected by the value of the resistivity. Second, the coexistence of the edge precursors and the core collapse in the experiment can be reasonably explained by the simulation result. The core collapse is not directly caused by the linear mode activities, but results from the flattening of the pressure gradient due to the disordering of the magnetic structure. Under this scenario, the role of the precursor modes is only to trigger the flushing of the core pressure. The magnitude and the time constant of the collapse are governed by global parameters such as the pressure gradient. Third, the experimental observation that only the density drops, leaving the temperature profile unchanged, appears to show that the process is governed not by a conductive process, but by a convective one. The

simulation, which solves an almost pure convective process, supports that observation.

In summary, we have demonstrated the nonlinear dynamics of a heliotron plasma with a large pressure gradient during a collapse event induced by a ballooning-like resistive instability with an intermediate wave number. It is clear that the flushing of the core pressure is triggered by edge instabilities through the disordering of the magnetic field structures. The simulation result provides us with a basic understanding of the nonlinear behavior of the resistive modes. The identification of the mode structures between the experiment and simulation is a subject of our ongoing research. The recent stability analysis for the LHD-SDC plasma [7] shows that the configuration is almost stable for the ideal modes. Therefore, control of the resistive modes will be important. More systematic analyses of the resistive modes will be performed in the next step of this study.

This work was presented at the 22nd IAEA Fusion Energy Conference (Geneva, 2008, TH/P9-17) and will be published in *Nuclear Fusion* [8] in more detail.

Naoki Mizuguchi National Institute for Fusion Science Toki, Gifu 509-5292, Japan E-mail: mizu@nifs.ac.jp

References

- [1] N. Ohyabu et al., Phys. Rev. Lett. 97, 55002 (2006).
- [2] R. Sakamoto et al., Plasma Fusion Res. 2, 047 (2007).
- [3] S. Ohdachi et al., 22nd IAEA Fusion Energy Conf., (Geneva, 2008) EX/8-1Rb.
- [4] K. Harafuji et al., J. Comput. Phys. **81**, 169 (1989).
- [5] Y. Suzuki et al., Nucl. Fusion. 46, L19 (2006).
- [6] N. Mizuguchi et al., Nucl. Fusion 47, 579 (2007).
- [7] Y. Narushima et al., Joint Conf. 17th Int. Toki Conf. and 16th Int. Stellarator/Heliotron Workshop (Toki, 2007), P1-053.
- [8] N. Mizuguchi et al., Nucl. Fusion **49**, to be published (2009).

All Wendelstein 7-X coils successfully tested

The last of the superconducting Wendelstein 7-X (W7-X) coils has successfully passed cryogenic tests at CEA Saclay near Paris. The 50 non-planar and 20 planar coils of W7-X are the heart of the device and technically the most demanding components. The non-planar coils produce the helically twisted magnetic field, responsible for the confinement of the plasma. For experimental flexibility, the radial plasma position and the helical twist of the magnetic field lines can be modified by the planar coils.

In 1998, the contract for the production of the non-planar coils was placed with a consortium of two companies, Babcock-Noell in Germany and Ansaldo in Italy. The planar coils were manufactured by TESLA in the UK. The production of the coils went through many ups and downs: various technical problems, in particular with the electrical insulation, had to be solved during the production; but also quite substantial modifications, especially on the casings and the support blocks, have been implemented. During the cold tests in Saclay the superconductor performed better than expected, showing no degradation due to bending inside the coils or welding of the aluminium alloy jacket. However, the electrical insulation of the non-planar coils in the header area, where the winding pack layers are connected and the connections to the power supplies are made, had to be reworked on several coils.

The tests at Saclay demonstrated that the specifications were achieved. The tests at around 5.7 K included several current cycles. For each coil type at least one temperature-induced quench was provoked by increasing the temperature to at least 6.2 K until the conductor quenched. In addition to confirming that the coils achieved the specified current and the thermally induced quench safety margin, the thermal cycles revealed weaknesses of the electrical insulation. Subsequent high-voltage tests at Paschen conditions showed in such cases breakthrough voltages below the specified values. After reworking of the critical areas, the necessary voltages could be achieved for all coils.

Completing the acceptance test, the last non-planar coil was used to experimentally verify the stability of the cable-in-conduit superconductor with respect to mechanical disturbances. An open question with respect to the W7-X design was whether the energy released during possible stick-slip events, originating from the sliding elements within the extremely highly loaded mechanical support structure, could in the worst case induce a quench in the superconducting cable. Therefore, qualification of the sliding support elements included mechanical tests to ensure a sufficiently large number of magnetic field load cycles without any stick-slip. In addition, the so-called mechani-

cal quench (MQ) test was developed to investigate the effect of such a stick-slip in case it still occurs in spite of all the precautions (Fig. 1). The MQ test assembly consisted of a pendulum which, via a transfer rod, applied a defined energy to the electrically charged coil inside the cryostat. The amplitudes and the frequency spectrum of the impact response were calculated to be comparable to the various stick-slip possibilities in the coil support elements. The results of this test are very comforting: even the highest impact energies corresponding to improbable simultaneous stick-slip events, combined with the lowest stability margin of the conductor expected during W7-X operation at a field of 3 T on-axis could not induce a quench. This suggests that even if stick-slip occurs, no quench of any superconducting coil is to be expected.

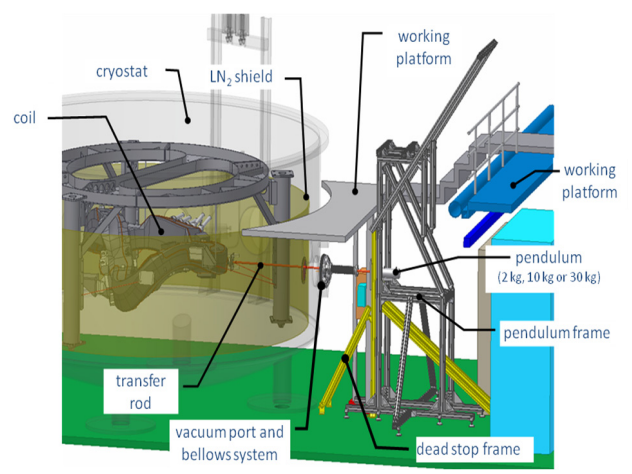


Fig. 1. MQ test setup. The superconducting coil is hit by different pendulum weights via a transfer rod that is fed through the cryostat wall and the thermal LN_2 -shield. The transfer rod is sealed against the cryostat wall with a double bellows system with intermediate vacuum. The pendulum, hanging from the pendulum frame, is released from different heights. The dead stop frame limits the movement of the transfer rod and the attached coil.

Altogether, the assembly of W7-X is progressing well. Some problems result from the extremely tight space conditions inside the cryostat, which require quite resource-intensive collision analyses regarding positioning of the helium pipe work and superconducting bus system, as well as the thermal superinsulation covering the inside of the outer cryostat vessel and the outside of the ports. Also, the application of the electrical insulation to the cable joints turned out to be much more difficult and time-consuming under real, very tight assembly conditions as compared to the qualification of these assembly steps at the work bench. At present, assembly work is progressing on four of the five magnet modules. Figure 2 shows the torus hall and the current state of assembly.

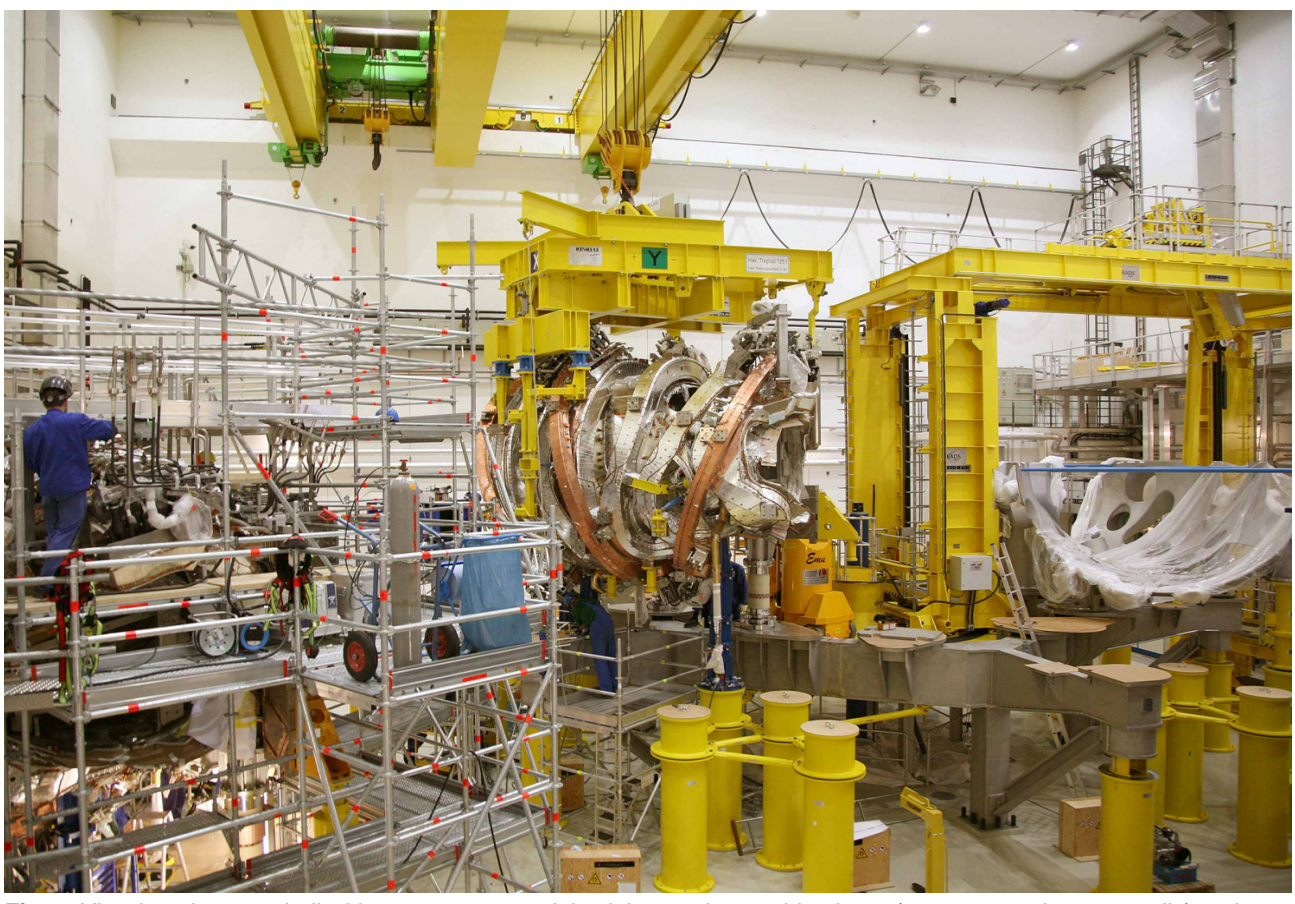


Fig. 2. View into the torus hall with one magnet module sitting on the machine base (at present only temporarily) and another one alongside. On the right one lower shell of the outer cryostat vessel can be seen.

W7-X Newsletter:

Coordination: Prof. a. D. Dr. Robert Wolf
Contact: Dr. Andreas Dinklage
E-mail: andreas.dinklage@ipp.mpg.de